Physics Letters A 376 (2012) 179–184

Contents lists available at SciVerse ScienceDirect

Physics Letters A

www.elsevier.com/locate/pla

First-principles study of the structural, magnetic, and electronic properties of $LiMBO_3$ (M = Mn, Fe, Co)

Zhiping Lin [a,b], Yu-Jun Zhao [a], Yanming Zhao [a,*]

[a] Department of Physics, South China University of Technology, Guangzhou 510640, China
[b] School of Physics, Guangdong University of Technology, Guangzhou 510090, China

ARTICLE INFO

Article history:
Received 23 March 2011
Received in revised form 28 July 2011
Accepted 9 August 2011
Available online 10 September 2011
Communicated by R. Wu

Keywords:
First-principles calculation
Lithium metal borate
Magnetism
Electronic structure

ABSTRACT

We present a first-principles calculation for the structural, magnetic, and electronic properties of $LiMBO_3$ (M = Mn, Fe, Co). Along the [0 0 1] direction, transition metals shows antiferromagnetic coupling in $LiMBO_3$ of both hexagonal and monoclinic lattices. The calculated magnetic moment of $5\mu_B$ per formula unit is close to the experimental value. These compounds are semiconductors with band gap of 0.4–2 eV, and with average intercalation voltages of 2–4.8 V.

1. Introduction

Along with the demonstration of reversible electrochemical lithium insertion–extraction for $LiFePO_4$ in 1997 [1], lithium transition metal phosphate with olivine structure $LiMPO_4$ (M = Fe, Mn and Co) have attracted much attention as new cathode materials of Li-ion batteries [2–4]. In phospho-olivines, the oxygen ions form strong covalent bond with P^{5+} to build the $PO_4{}^{3-}$ tetrahedral polyanion. These polyanions enable low transition metal redox energies through the inductive effect [1,5–9]. On the other hand, polyanions also bring some inactive mass that impedes both the specific capacity and the specific energy. Up to now, most of the studies focus on the effect of the nature of the polyanion utilizing tetrahedral groups $(XO_4)^{2-}$ or $(XO_4)^{3-}$ with X = S, P or V [1–12]. Recently, Li_2O–MO–B_2O_3 (M = Mn, Fe, Co) have attracted some attentions as electrode materials for lithium batteries, and give a preliminary evaluation of the inductive effect [13,14]. The structure of $LiMBO_3$ (Fe, Co, Mn, Mg and Zn) is built by MO_5 trigonal bipyramids and BO_3 planers to form the three-dimensional $[MBO_3]_n{}^{n-}$ framework. The electrochemical study shows that only a small amount of lithium can be deinserted reversibly from the compounds [15]. From the thermodynamic study performed in the case of $LiFeBO_3$, the Fe^{3+}/Fe^{2+} reduction couple lies between 3.1 and 2.9 V/Li, demonstrating an important inductive effect of the BO_3 group. Recently, Zhao group have synthesized $LiFeBO_3$ successfully by solid state reaction method [14]. Results show that the initial specific capacity is 125.8 mA h/g under the discharge current density of 5 mA/g. When the discharge current density is increased to 50 mA/g, the specific capacity of 88.6 mA h/g can still be held. The $LiMnBO_3$ has been synthesized and show the initial specific discharge capacity was 75.5 mA h/g at the current density of 5 mA/g and the mean fade of capacity was 0.09% per cycle except for the first cycle [16]. The $LiMnBO_3$ has two structures: the monoclinic structure isotypic with $LiFeBO_3$ and the hexagonal structure isotypic with the hexagonal form of $LiCdBO_3$. For mono-$LiMnBO_3$, each MnO_5 bipyramid shares two edges with the adjacent bipyramid to single chains and the planar BO_3 groups link three chains via corner sharing as shown in Fig. 1(a), indicating that Mn and Li atoms occupy two nearby positions uniformly. For h-$LiMnBO_3$, each MnO_5 square pyramid shares two opposite edges of its square base with two adjacent pyramids and planar BO_3 groups link three chains via corner sharing (shown in Fig. 1(b)). Up to now, the study about the electronic structure and band gap of lithium metal borate is scarce. Hence, in this Letter, we investigate the structural, magnetic, and electronic properties, as well as the average intercalation voltage in $LiMBO_3$ (M = Mn, Fe and Co) using first-principles calculations.

2. Computational details

The calculations are based on density-functional theory with the general gradient approximation (GGA) using Perdew–Wang form for the exchange correlation energy [17] as implemented in

* Corresponding author. Tel.: +86 020 87111963.
E-mail addresses: zhipinglphy@gdut.edu.cn (Z. Lin), zhaoym@scut.edu.cn (Y. Zhao).

0375-9601/$ – see front matter
doi:10.1016/j.physleta.2011.08.018

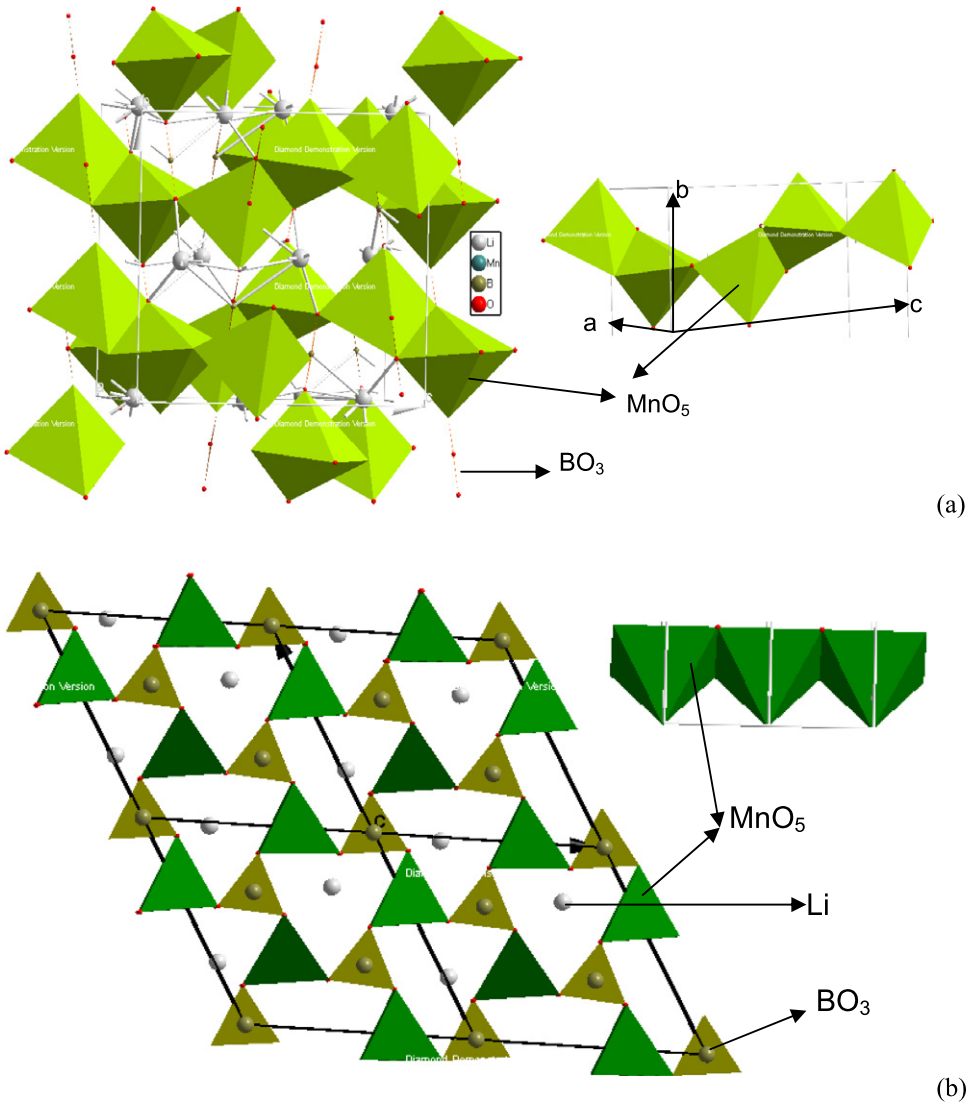

Fig. 1. The three-dimensional framework of $LiMnBO_3$: (a) monoclinic structure; and (b) hexagonal structure.

the Vienna Ab Initio Simulation Package (VASP) [17,18]. The GGA approximation was adopted and the electron–ion interactions were described by the PAW pseudopotentials. The wave functions are expanded in plane waves with an energy cutoff of 500 eV. Brillion zone integration of band structure is performed with $2 \times 2 \times 5$ Monkhorst–Pack mesh for monoclinic structure and $4 \times 3 \times 2$ for hexagonal structure. The formation energies are well converged with respect to k-points within 10^{-3} eV. Fermi level is smeared by the Gaussian method with a width of 0.1 eV. In order to obtain the orbital-projected electronic structure information, the Wigner–Seitz radii of 0.80, 1.00, 0.40 and 1.40 for Li, Mn, B and O ion are adopted, respectively.

The average Li insertion potential could be obtained through total energy calculations [19,20]. If ΔG_r is the Gibbs free energy for the reaction:

$$MnBO_3\,(\text{cathode}) + Li\,(\text{anode}) \rightarrow LiMnBO_3\,(\text{cathode}).$$

The average insertion voltage is given by

$$\bar{V} = -\frac{\Delta G_r}{F}, \tag{1}$$

where F is the Faraday constant. Since the effects due to changes in volume and entropy are negligible, the Gibbs energy difference is approximated by the internal energy difference at 0 K, supplied by our first-principles total-energy calculations through

$$\Delta E_r = E_{LiMBO_3} - E_{Li} - E_{MBO_3}. \tag{2}$$

Here the cohesive energy of Li is calculated in its bcc structure, which corresponds to the structure phase of the Li anode.

3. Results and discussion

All the lattice parameter calculations are performed by the GGA approximation, which usually leads to lattice parameters in good agreement with experiment. Since the effect of spin polarization was found to be essential, non-magnetic (NM), ferromagnetic (FM) and antiferromagnetic (AFM) arrangement of the transition metal ions are considered in the calculations. We first consider the possible magnetic coupling along the c-direction of h-$LiMnBO_3$. The calculated results (cf. Table 1) indicate that AFM configuration with spin orientation alternatively changed along c-direction (as shown in Fig. 2(a)) is energetically favored, in agreement with the experimental result that 1D AFM interactions within the MnO chains dominate the magnetic coupling above 47 K [21]. The distance of Mn–Mn along c-direction (3.147 Å) is shorter than that of Mn–Mn in ab-plane, and indicates the strong AFM coupling between

Table 1
The parameters, energies and volumes of $LiMnBO_3$ with two different structures. Experimental values are given as in Ref. [16].

		a (Å)	b (Å)	c (Å)	β	V (Å^3)	E_0 (eV)
h-$LiMnBO_3$	Expt.	8.1720		3.1473		182.02	
	NM	7.9766		2.9020		161.27	−42.563
	FM	8.2355		3.1499		185.15	−44.752
	AFM_c	8.2477		3.1253		183.97	−44.794
	AFM_ab	8.3119		3.0355		181.40	−45.022
Mono-$LiMnBO_3$	Expt.	5.1880	8.9520	10.3670	91.75	481.25	
	NM	5.2702	8.6073	10.2148	90.45	455.86	−42.932
	FM	5.2301	8.6253	10.8146	90.33	482.78	−43.844
	AFM	5.2102	8.7352	10.8912	90.52	490.72	−44.066

Table 2
The optimized Wyckoff coordinates, parameters and volumes of h-$LiMnBO_3$ and its delithium phase $MnBO_3$.

	$LiMnBO_3$ (Calc.)	$LiMnBO_3$ (Expt.[a])	$MnBO_3$ (Calc.)
a (Å)	8.2477	8.1720	8.3101
c (Å)	3.1253	3.1473	2.9458
V (Å^3)	183.97	182.02	172.42
Li	(0.0130, 0.3008, 0.5124)	(0.0191, 0.3031, 0.5000)	–
Mn	(0.3680, 0.3598, 0.0068)	(0.3708, 0.3589, 0.0000)	(0.3700, 0.3630, −0.0007)
B_1	(0.3330, 0.6667, 0.5170)	(0.3333, 0.6667, 0.5000)	(0.3337, 0.6670, 0.5194)
B_2	(0.0005, 0.0000, 0.0172)	(0.0000, 0.0000, 0.0000)	(0.0014, 0.0013, 0.0186)
B_3	(0.6665, 0.3334, 0.5149)	(0.6667, 0.3333, 0.5000)	(0.6654, 0.3321, 0.5098)
O_1	(0.1398, 0.5762, 0.5220)	(0.1389, 0.5808.0.5000)	(0.1454, 0.6127, 0.5184)
O_1	(0.1098, 0.9168, 0.0144)	(0.1162, 0.0780, 0.0000)	(0.0740, 0.8829, 0.0233)
O_3	(0.7472, 0.2212, 0.5186)	(0.7505, 0.2227, 0.5000)	(0.7247, 0.1996, 0.5074)

[a] Ref. [13].

Mn–Mn. According to the report by Li et al., the Mn atoms spin configuration in *ab*-plane is noncollinear with a mixture of one FM Mn triangle and two normal 120° AFM Mn triangles (the Mn–Mn bond length for three different Mn_3 triangles is 4.368 Å-B3, 4.643 Å-B1 and 5.178 Å-B2, respectively) in a magnetic supercell with 108 atoms [21].

A novel chiral AFM coupling in the *ab*-plane of h-$LiMnBO_3$ was reported under a lower temperature (e.g. 28.5 K) through magnetic neutron diffraction measurement, according to Ref. [21]. Since the noncollinear ordering calculation takes much computational resources, it is difficult to simulate the chiral AFM ordering in *ab*-plane with possible AFM coupling along *c*-direction (a larger supercell is required). Here, we calculated the total energy of h-$LiMnBO_3$ of chiral AFM coupling in *ab*-plane (as shown in Fig. 2(b)) and FM coupling along *c*-direction. It is found to be lower by 0.228 eV than that of collinear AFM configuration along *c*-direction. The detailed magnetic order in *ab*-plane simulated here is a noncollinear magnetic ground state with a mixture of one FM Mn triangle and two normal 120° AFM Mn triangles. This clear indicates that the ground state of the magnetic ordering in *ab*-plane could be the experimentally reported chiral AFM coupling.

The spin polarization results of mono-$LiMnBO_3$ system are also listed in Table 1. It indicates that mono-$LiMnBO_3$ is also a compound with AFM structure. To gain further insight into the possibility of antiferromagnetism, we calculated all the possible collinear configurations. From theoretical total energies for all studied spin configurations, we find that the AFM spin configuration along *c*-direction is the magnetic ground state of mono-$LiMBO_3$, as shown in Fig. 2(c). Our calculated results also show that, as mono-$LiMnBO_3$, $LiFeBO_3$ and $LiCoBO_3$ systems with monoclinic phase have the one dimension antiferromagnetic along *c*-direction.

The calculated parameters and volumes with spin polarization are listed in Table 1. It is clear that the parameters and volume of the systems are improved when the spin polarization is considered. In h-$LiMnBO_3$ structure, the errors of the calculated volumes of the unit cell are only 1.7% (FM), 1% (AFM_c) and 0.3% (AFM_ab) comparing with experimental values, respectively. Meanwhile, the calculated volumes of the unit cell of mono-$LiMnBO_3$ structure increase 0.3% (FM) and 1.9% (AFM). The computed parameters of spin polarization are also in agreement with experimental values. Hence, the magnetic interaction is important for the characteristic of $LiMBO_3$ (M = Mn, Fe, Co). The optimized Wyckoff coordinates of h-$LiMnBO_3$ as well as that of its delithiated structure listed in Table 2 are in good agreement with the experimental values. It is interesting to note that, for hexagonal structure, the lattice parameters and the Mn–O and P–O bond lengths of $MnBO_3$ change slightly with respect to $LiMnBO_3$: lattice parameters change by 2.9% and 4.5%, and the bond lengths of Mn–O and P–O change by 0.5% and 0.6% on the average, respectively. For monoclinic phase, the calculated lattice unit cells have distinctly distorted compared with experimental results. In addition, our results show that the volume changes with 4.95% (hexagon) and 5.58% (monoclinic) upon Li extraction from $LiMnBO_3$ to $MnBO_3$ is small. It is obvious that the good structure stability of $LiMBO_3$ favors its electrochemical performance when it is used as cathode material of lithium-ion battery.

Fig. 3 shows the total density of state of h-$LiMnBO_3$ under different spin polarization. The non-spin configuration shows metal characteristics since its Fermi level lies within the Mn 3d band. The spin-polarized h-$LiMnBO_3$ is demonstrated to be semiconductor. The width of band gap is 1.46 eV (Fig. 3(a)) for FM spin configuration, 1.73 eV (Fig. 3(c)) for AFM spin configuration along *c*-direction, and 1.90 eV (Fig. 3(b)) for the chiral magnetic ground state within the *ab*-plane, respectively. The band gap shown in Fig. 3(b) is the widest and this magnetic configuration is the most stable experimentally and theoretically. In Fig. 4, we show the electron density of states for mono-$LiMBO_3$ (M = Mn, Fe, Co) with AFM spin structure, which is determined by more accurate GGA + U method with U = 4. The GGA + U approach usually improves the treatment of correlation effects in localized orbital that are formed by the metal 3d orbital and oxygen 2p lagans. In GGA + U, local atoms like 3d states are projected out and treated with a Hubbard model. Therefore, this method makes more ap-

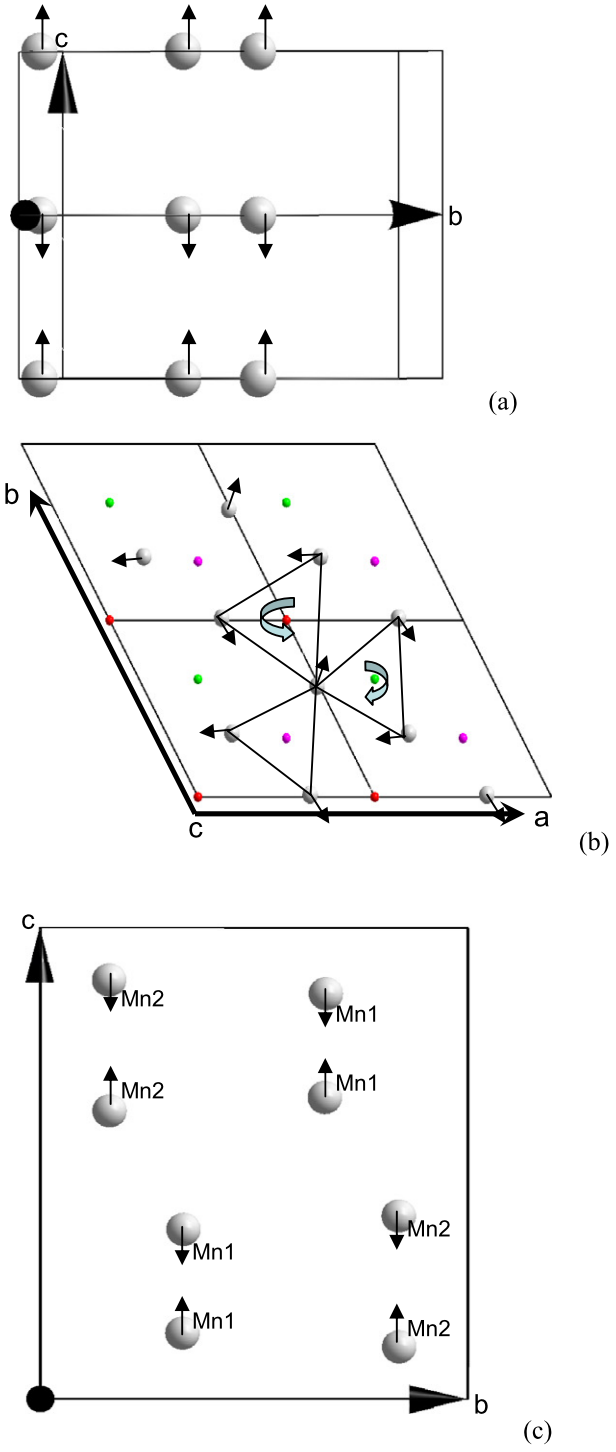

Fig. 2. The magnetic structure of $LiMnBO_3$: (a) AFM arranged Mn along *c*-direction in h-$LiMnBO_3$; (b) the chiral magnetic ordering of Mn in *ab*-plane of h-$LiMnBO_3$; (c) AFM arranged Mn along *c*-direction in mono-$LiMnBO_3$. Here, Mn is denoted by the silver balls, while B_1, B_2, and B_3 are shown with green, red, and pink balls. (For interpretation of the references to color in this figure legend, the reader is referred to the web version of this Letter.)

plicable to transition metal compound to correct the energies and to improve the bands and magnetic moments. For example, in the case of $LiFePO_4$ the calculated band gap from GGA lies the range 0–0.3 eV, but the GGA + U result is about 3.7 eV that is close to the measured value from diffuse reflectance spectroscopy [22]. From Fig. 4, it can be seen that the band gap lies 0.39–2.0 eV for mono-$LiMBO_3$ (M = Mn, Fe, Co). Thereinto, the band gap of Co compound is the smallest and that of Mn compound is the largest

Table 3
The formation enthalpy of Li vacancy in h- and mono-$LiMnBO_3$. Li_1 and Li_2 denote two different lithium ions in the monoclinic structure, which occupy statistically two close position with the occupancy of 50% for Li_1 and 50% for Li_2, respectively.

	Li (h-$LiMnBO_3$)	Li_1 (mono-$LiMnBO_3$)	Li_2 (mono-$LiMnBO_3$)
ΔH (eV)	−1.703	−1.500	−1.432

under the same U value. All these compounds of ground states show semiconducting, in good agreement with the experimental result of electronic conductivity measurement [14,16].

The $LiMnBO_3$ is formed by the three-dimensional $[MBO_3]_n^{n-}$ framework. When Li is de-intercalated from the compound, it will create a Li vacancy. Due to Li atoms located in different lattice locations, there is one type of Li vacancy for h-$LiMnBO_3$ and two types of Li vacancies for mono-$LiMnBO_3$. Two types of Li atoms in mono-$LiMnBO_3$ occupy statistically two close positions with the occupancy of 50% for Li_1 and 50% for Li_2, respectively. The formation enthalpies for different Li vacancies have been computed (listed in Table 3) by

$$\Delta H(\text{Li vacancy}) = E(\text{LiMnBO}_3) - E(\text{Li}_x\text{MnBO}_3) - (1-x)E(\text{Li}).$$

The results demonstrate that the formation enthalpy of Li vacancy for h-$LiMnBO_3$ compound is lower than that of monoclinic $LiMnBO_3$ compound. Hence, the extraction of lithium in h-$LiMnBO_3$ compound is easier than that in the monoclinic structure compound. For mono-$LiMnBO_3$, vacancy formation energies of two kinds of Li vacancies are different. Vacancy located in Li_1 can be formed easier than that of Li_2, and the formation energies of two different vacancies is low and then the extraction of two type's lithium ions is also very easy theoretically.

One of the critical properties for a Li intercalation material is the potential at which Li can be removed and inserted. The theoretical average intercalation voltages are also calculated through Eqs. (1) and (2) and total energy for $LiMBO_3$ by GGA + U approximation, as listed in Table 4. The calculated average intercalation voltage of 4.59 V for h-$LiMnBO_3$ agrees well with that located between 2 and 4.8 V obtained by experimental measurement [13,16]. The intercalation voltage of monoclinic structure $LiMnBO_3$ is 4.65 V that is close to that of h-$LiMnBO_3$. Therefore, our result suggests that the difference in symmetry of the two intercalated phases has little influence on the intercalation voltage. According to the calculated results, it is clear that in the h-$LiMnBO_3$ structure, along with the extraction of lithium the internal relaxation keeps the MnO_5 square pyramid perfect and there is a reduction of volume and lattice parameters. When lithium is extracted from the compound, metal–oxygen bond length will change (listed in Table 5). The average Mn–O bond length around Mn^{3+} site is decreased to 1.989 Å comparing to 2.132 Å surrounding the Mn^{2+} sites. It implies that there are greater electronic repulsions between Mn and O square pyramid. Then, the bond length among Mn and O becomes larger and the total equilibrium volume of the cell increase along with the insertion of Li by electrostatic repulsion effects. Wolverton et al. [23] and Aydinol et al. [20] have proposed that not only Co but also O is oxidized with the removal of Li in $LiCoO_2$. This suggested that the Co ion undergoes a charge transfer: its oxidation state changes from Co^{3+} in $LiCoO_2$ to Co^{4+} in CoO_2. In the case of $LiFePO_4$, the same phenomenon is also observed experimentally and theoretically [24]. In h-$LiMnBO_3$ compound, along with Li intercalation the net charge of the oxygen ion decreases from 6.572e to 5.589e. Hence, the net electron transfer induced by the Li intercalation is predominantly to oxygen, not to metal.

4. Conclusion

Our calculated results reveal that spin polarization plays an essential role in stabilizing the electronic states of $LiMBO_3$ (M = Mn,

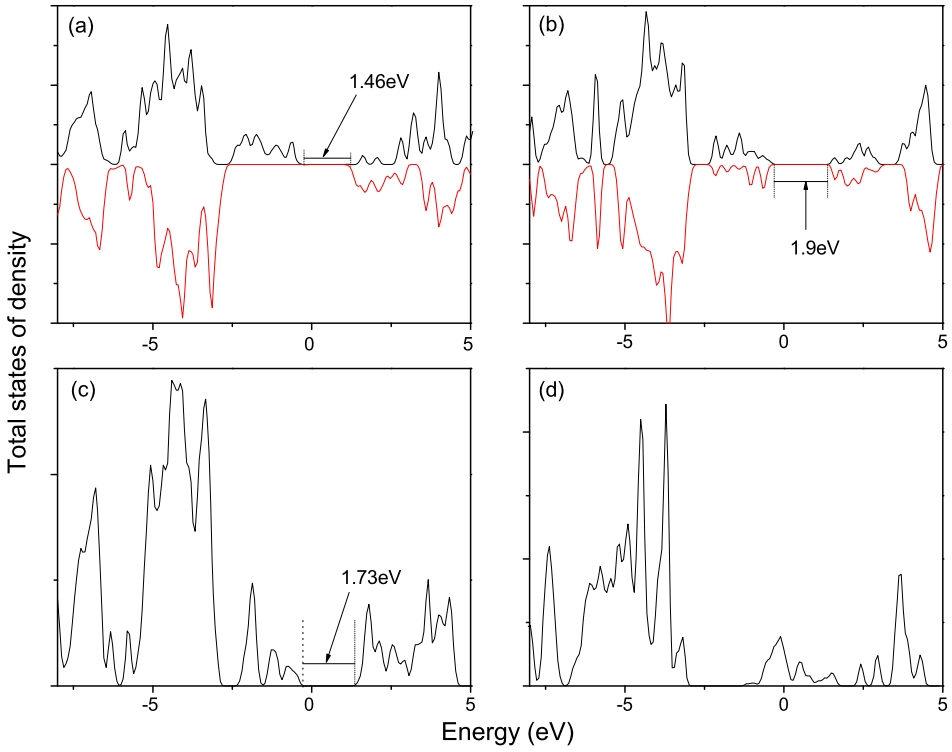

Fig. 3. The total density of state of h-$LiMnBO_3$ with Mn atoms arranged by (a) FM; (b) noncollinear chiral AFM in *ab*-plane; (c) 1D collinear AFM along *c*-direction; as well as (d) non-magnetic.

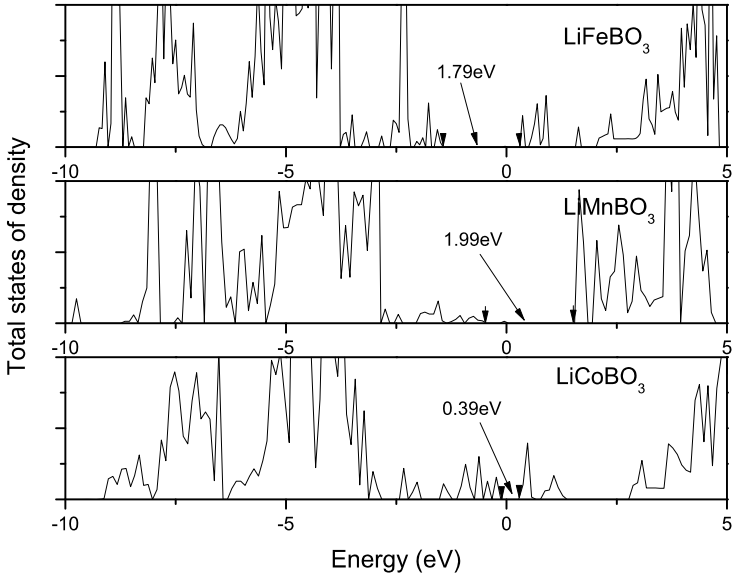

Fig. 4. The total density states of mono-$LiMBO_3$ (M = Co, Fe, Mn) under GGA + U with U = 4.

Table 4
Calculated average intercalation voltage for h- and mono-$LiMBO_3$ (M = Mn, Fe, Co) by GGA + U, where U = 4.

	h-$LiMnBO_3$	Mono-$LiMnBO_3$	Mono-$LiFeBO_3$	Mono-$LiCoBO_3$
Voltage (V)	4.59	4.65	3.82	2.96

Fe, Co). For $LiMnBO_3$ compound, not only hexagonal lattice but also monoclinic lattice show the AFM coupling along the [0 0 1] direction when collinear magnetic ordering is considered. The calculated magnetic moment of $5\mu_B$ per formula unit is close to the experimental value. The calculated total energy of h-$LiMnBO_3$ with noncollinear chiral AFM coupling in *ab*-plane and FM coupling along *c*-direction is lower than the collinear AFM along *c*-direction. This clearly supports the experimental observation of the novel chiral magnetic ground state in *ab*-plane under lower ordering temperature (28.5 K). For Fe and Co compounds, the ground state of magnetism is one-dimensional AFM along *c*-direction under the collinear magnetic ordering simulation. The density of states of

Table 5
The bonding lengths of Mn–O, B–O, and Li–O in h-$LiMnBO_3$ and $MnBO_3$ structures. The $\times 2$ or $\times 3$ expresses that the same length have two or three.

Compounds		Mn–O	B–O	Li–O
$LiMnBO_3$	Cal.	2.059, 2.142 × 2, 2.159 × 2	1.390 × 3	1.950, 1.975, 1.983 × 2
	Expt.	2.078, 2.154 × 2, 2.169 × 2	1.381, 1.383, 1.379	1.951, 1.972, 1.982 × 2
$MnBO_3$	Cal.	1.853, 2.000 × 2, 2.046 × 2	1.380 × 3	

these compound with AFM along [0 0 1] direction shows that these compounds are semiconductors with the band gaps of 0.4–2 eV. The corresponding calculated voltage of 2–4.8 V is in agreement with the experimental value.

Acknowledgements

This work was funded by NSFC Grants (Nos. 50772039 and 10704025) through NSFC Committee of China and the Foundation (No. S2011020000521) through the Science and Technology Bureau of the Guangdong Government respectively.

References

[1] A.K. Padhi, K.S. Nanjundaswamy, J.B. Goodenough, J. Electrochem. Soc. 144 (1997) 1188.
[2] K. Amine, H. Yasuda, M. Yamachi, Electrochem. Solid-State Lett. 3 (2000) 178.
[3] J. Carrasco, N. Lopez, F. lllas, Phys. Rev. Lett. 93 (2004) 225502.
[4] A. Yamada, S.-C. Chung, J. Electrochem. Soc. 148 (2001) A960.
[5] A. Manthiram, J.-B. Goodenough, J. Solid State Chem. 71 (1987) 349.
[6] A.K. Padhi, K.S. Nanjundaswamy, C. Masquelier, S. Okada, J.B. Goodenough, J. Electrochem. Soc. 144 (1997) 1609.
[7] A.K. Padhi, K.S. Nanjundaswamy, C. Masquelier, J.B. Goodenough, J. Electrochem. Soc. 144 (1997) 2581.
[8] A.K. Padhi, W.B. Archibald, K.S. Nanjundaswamy, J.B. Goodenough, J. Solid State Chem. 128 (1997) 267.
[9] C. Masquelier, A.K. Padhi, K.S. Nanjundaswamy, J.B. Goodenough, J. Solid State Chem. 135 (1997) 228.
[10] S. Okada, K.S. Nanjundaswamy, A. Manthiram, J.B. Goodewough, H. Ohtsuka, H. Arai, J. Yamaki, in: Proceedings of the 36th Power Sources Conference, 1994, p. 110.
[11] S.-C. Yin, H. Grondey, P. Strobel, M. Anne, L.F. Nazar, J. Am. Chem. Soc. 125 (2003) 10402.
[12] P. Fu, Y.M. Zhao, X.N. An, Y.Z. Dong, X.M. Hou, Electrochem. Acta 52 (2007) 5281.
[13] V. Legagneur, Y. An, A. Mosbah, R. Portal, A. Le Gal La Salle, A. Verbaere, D. Guyomard, Y. Piffard, Solid State Ionics 139 (2001) 37.
[14] Y.Z. Dong, Y.M. Zhao, Z.D. Shi, X.N. An, P. Fu, L. Chen, Electrochem. Acta 53 (2008) 2339.
[15] Y. An, V. Legagneur, A. Mosbah, R. Portal, A. Le Gal La Salle, A. Verbaere, D. Guyomard, Y. Piffard, Solid State Ionics 139 (2001) 37.
[16] Ling Chen, Yanming Zhao, Xiaoning An, Jianmin Liu, Dong Youzhong, Yinghua Chen, Quan Kuan, J. Alloys Comp. 494 (2010) 415.
[17] G. Kresse, J. Joubert, Phys. Rev. B 59 (1999) 1758.
[18] G. Kresse, J. Hafner, Phys. Rev. B 47 (1993) 558;
G. Kresse, J. Hafner, Phys. Rev. B 49 (1994) 14251;
G. Kresse, J. Hafner, J. Phys.: Condens. Matter 6 (1994) 8245;
G. Kresse, J. Furthmůller, Comput. Mater. Sci. 6 (1996) 15;
G. Kresse, J. Furthmůller, Phys. Rev. B 54 (1996) 11169.
[19] G. Ceder, M.K. Aydinol, A.F. Kohan, Comput. Mater. Sci. 8 (1997) 161.
[20] M.K. Aydinol, A.F. Kohan, G. Ceder, K. Cho, J. Joannopoulos, Phys. Rev. B 56 (1997) 1354.
[21] R.K. Li, C.T. Chen, C. Greaves, Phys. Rev. B 66 (2002) 052405.
[22] Fei Zhou, Kisuk Kang, Thomas Maxisch, Gerbrand Ceder, Dane Morgan, Solid State Commun. 132 (2004) 181.
[23] C. Wolverton, A. Zunger, Phys. Rev. Lett. 81 (1998) 606.
[24] S.Q. Shi, L.J. Liu, C.Y. Ouyang, D.S. Wang, Z.X. Wang, L.Q. Chen, X.J. Huang, Phys. Rev. B 68 (2003) 195108.